LAWRENCE
LIVERMORE
NATIONAL
LABORATORY

LLNL-JRNL-663392

Estimation of excited state absorption and photo-bleaching in Fe2+ doped lithium sodium silicate glass under exposure to high power nanosecond laser pulses

S. G. Demos, P. R. Ehrmann, S. Qiu, K. I. Schaffers, T. I. Suratwala

October 29, 2014

Optics Express

Disclaimer

Estimation of excited state absorption and photo-bleaching in Fe^{2+} doped lithium sodium silicate glass under exposure to high power nanosecond laser pulses

Stavros G. Demos*, Paul R. Ehrmann, S. Roger Qiu, Kathleen I. Schaffers, Tayyab I. Suratwala

Lawrence Livermore National Laboratory, 7000 East Avenue, Livermore, CA 94551, USA

*demos1@llnl.gov

Abstract: Representative samples of Fe-doped lithium sodium silicate glasses co-doped with Sn and C to promote the Fe^{2+} redox state are investigated under simultaneous excitation at the first and third harmonics of a nanosecond Nd:YAG laser. The aim is to evaluate critical parameters associated with the potential use of this material as optical filter that transmits the third harmonic but blocks the fundamental frequency. Estimations of the excited state absorption coefficient and photobleaching (reduction of absorption at the fundamental) are provided. Although the materials examined are not ideal for the intended application, the results provide insight on the design and expected operational parameters of such optimized materials.

Introduction

A number of large-aperture high power or high peak intensity lasers are currently under development to complement a short list of existing systems. The development of these systems, which devoted to fundamental physics and material characterization at extreme conditions, has been enabled in large part by advances in manufacturing of large aperture optical materials. Glass based materials represent a robust and relatively inexpensive solution to manufacture various types of optical components for such laser systems [1]. Ion-doped glass material are incorporated in various components such as for laser glass, ultraviolet light filtering glass for laser flashlamps and in various types of diffractive optical components to improve performance (such as to reduce solarization) [1].

Iron ions are typically found in glass materials as a contaminant but Fe^{2+} and Fe^{3+} ions incorporated in various glass and crystalline matrixes provide characteristic optical absorption spectra [2-8]. These spectra are dependent on the oxidation state of the Fe ions [9-11] and also on the symmetry and crystal field strength [12-14]. In silicate glasses, the Fe ions (in both oxidation states) occupy octahedral and tetrahedral sites while the Fe redox ratio (the relative concentration of the Fe^{2+} and Fe^{3+} ions) is typically influenced by the melting temperature and incorporation of oxidizing or reducing agents. Fe^{3+} ions typically introduce absorption bands in the visible and near ultraviolet range while the ultraviolet (UV) absorption edge arises from charge transfer absorption bands. Similarly, the UV absorption edge from Fe^{2+} ions arises from charge transfer absorption peaks but is typically slightly blue-shifted. In addition, Fe^{2+} ions introduce a broad absorption band in the near infrared (NIR) region.

The absorption characteristics of Fe^{2+} impurity ions provide the basis for their incorporation in NIR absorbing glass filters that can exhibit (in the absence of Fe^{3+} ions) high transmission in the visible spectrum. Here we consider the possibility that Fe^{2+} doped glass may be suitable as NIR absorbing filter in large aperture, high power laser systems suitable for transmitting with very low losses the third harmonic of the system (typically based on Nd:glass laser material) while significantly reducing the fundamental frequency which is located in the NIR spectral region. Such laser systems generate pulses with temporal duration on the order of 1 to 10 ns and convert the fundamental frequency to the third harmonic, which is subsequently used to irradiate the target. However, there may be significant amount of unconverted light (at the fundamental frequency) that may be desirable to be impeded from reaching the target. While there are various designs to perform this task, using a "red blocking" filter is a possible viable method.

This work focuses on examining the operation of Fe^{2+} doped glass samples under simultaneous exposure to high fluence excitation conditions at the fundamental (1064 nm) and the third harmonic (355 nm) of an Nd:YAG laser. The aim is to investigate processes that may be limiting the performance of Fe^{2+} doped glass materials as "red blocker" materials in large aperture ns laser systems. These processes include excited state absorption, photo-bleaching and solarization. We also monitor the propagation of the laser beams for possible damage and self-focusing effects. While the samples are not ideal, they provide an initial evaluation for this combination of ion doping and base matrix for the intended application.

Experimental system

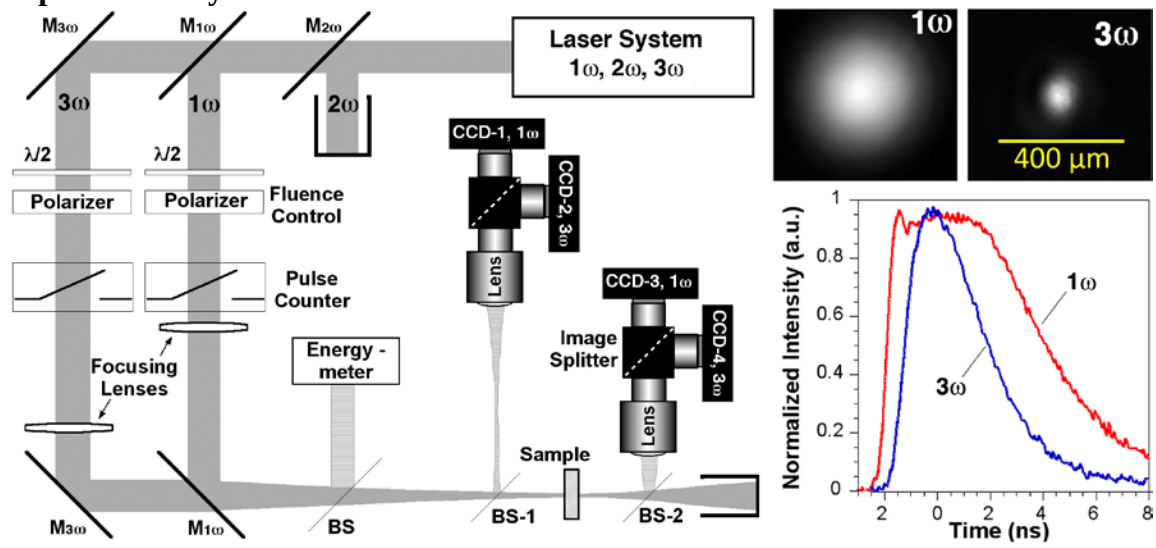

Fig. 1. Schematic depiction of the main components of the experimental system. 1ω, 2ω, 3ω: laser frequencies; $M_{1\omega}$, $M_{2\omega}$, $M_{3\omega}$: Dielectric 45° mirrors; BS: Beam splitter; CCD: Capturing the image of the beam profile of either the 1ω or 3ω beam at the plane corresponding to the exit surface of the sample. Inset shows the spatial and temporal characteristics of the 1ω and 3ω beams at the sample location.

The main components of the experimental system are shown in Figure 1. It involves a Nd:YAG laser system equipped with 2^{nd} and 3^{nd} harmonic generation nonlinear crystals that were tuned to provide sufficient power output 1064 nm and 355 nm (denoted as 1ω and 3ω, respectively). In this arrangement, the output of the laser contains all three wavelengths which are subsequently separated using dielectric mirrors. The 2ω component is not used in this work and is diverted into a beam dump. The temporal profiles of the 1ω and 3ω beams are shown as inset in Figure 1. The 3ω output pulses have a nearly Gaussian shape with temporal duration at full width at half maximum (FWHM) of about 3.3 ns. The 1ω pulse is flatter at the peak intensity (due to the nonlinear conversion of energy from 1ω to 2ω) and a temporal duration at FWHM of about 6 ns. The laser power and the pulse repetition rate were computer controlled and were adjusted as needed for the execution of the experiment. The repletion rate was set at 0.2 Hz to allow any thermal energy deposited in the location of laser exposure of the sample to diffuse in the material before the arrival of the next pulse.

The 1ω and 3ω beams are focused using 1-meter focal length (nominal) lenses located in the beam paths before the two beams were recombined. The position of the lenses was adjusted so that the focal point of each beam is positioned at the sample. The Raleigh length is estimated to be about 2 and 6 cm for the 3ω and 1ω beams, respectively. The samples were cut to about 1-3 mm thick sections so that their thickness is about an order of magnitude smaller than the Raleigh length to achieve a nearly collimated propagation of the focused beams through the sample.

Three fused silica plates are used to divert part of the combined 1ω and 3ω beams to 1) a power meter for pulse-to-pulse energy measurement, 2) to the reference beam diagnostic module and 3) to the output beam diagnostic module, as shown in Figure 1. These two beam diagnostic modules are identical and are composed of an imaging lens (providing about 6 X magnification) followed by an image splitter that directs each wavelength (1ω and 3ω beam) to a different CCD camera (denoted in Fig. 1 as CAM-1 and CAM-2 for the reference beam and CAM-3 and CAM-4 for the output beam modules). The output beam diagnostic modules provide the means to record the beam profiles at the output of the sample by imaging the output surface of the sample on each CCD camera. In this arrangement, the length of one pixel on the CCD camera corresponds to about 1 μm on the output surface of the sample. The reference beam diagnostic module is configured to record the beam profile at the same location (output surface of the sample) along the beam propagation path without the presence of the sample. This configuration facilitates monitoring in each wavelength the power and spatial profile of the beam at the plane corresponding to the output of the sample (with and without the sample) enabling an accurate determination of beam losses and modification due to linear and/or nonlinear processes as well as due to laser induced damage. Images of the beam profiles are shown in Figure 1 as inset. The beam radius at 1/e of peak intensity of about 48 μm for the 3ω beam and 124 μm for the 1ω beam.

A suitable set of filters was positioned in front of each CCD to attenuate the recorded intensity and remove the complementary wavelength. The filters of CAM-4 were exchangeable with a second set that allowed simultaneous visualization of both, the 1ω and 3ω beams. Visualization of both beam in this arrangement allowed aligning and overlapping the 1ω and 3ω beams on the sample using the stirring mirrors positioned

before the recombination of the beams. The beam-to-beam stability exhibited modulation in both, the spatial dimensions of the beam and at the location of the center of the beam. Specifically, the beam diameter modulation for the 3ω beam was on the order of 5 % and was associated with small changes in the lateral dimensions of the beam profile. The corresponding changes for the 1ω beam were smaller. In addition, the center of each beam moves around covering an area that has a diameter about twice that of the 3ω beam but this modulation was the same for both beams. Consequently, the two beams remained overlapped (after alignment) unaffected by the beam stability modulation effects.

Samples and Experimental protocol

The samples used in this work were down-selected from a series of glasses developed as part of a broader effort to develop a better understanding of how to control the oxidation state of Fe dopant ions in various glass hosts. Fe^{2+} doped glasses exhibit absorption characteristics potentially suitable for use as filters capable of absorbing the fundamental frequency of neodymium doped glass laser system (1053 nm) but allowing high transmission at the third harmonic (351 nm). Such a filter may be needed in high power laser systems for delivering to the target irradiation that does not contain the unconverted component of the fundamental frequency. The samples that were considered in this work were Fe doped Lithium Sodium Silicate glasses, containing various amounts of Sn and C co-doping to control the oxidation state. This glass material development work will be reported elsewhere [15].

In this work, we down-selected two representative samples based on their high Fe^{2+} (and low Fe^{3+}) concentration, the relatively better optical quality and uniformity and, the relatively higher laser induced damage threshold.

The first sample, henceforth referred to as “sample 1”, had nominal mol% composition 12.5 Li_2O-12.5 Na_2O-75 SiO_2 and Fe_2O_3=0.25 mol%, SnO=0.5 mol%, C=0 mole%. The sample had a thickness of about 1.9 mm and lateral dimensions of about 4 cm × 4 cm. Its damage threshold at 1ω and 3ω was about 10 J/cm^2 and 1.5 J/cm^2, respectively. The optical uniformity of the sample was adequate to perform the measurements causing minimal distortion of the beam profile. The second sample, henceforth referred to as “sample 2”, had nominal mol% composition 12.5 Li_2O-12.5 Na_2O-75 SiO_2 and Fe_2O_3=0.6 mol%, SnO=0.6 mol%, C=0.36 mole%. The sample had a thickness of about 2.84 mm with lateral dimensions of about 3 cm × 3.5 cm. The damage threshold at 1ω and 3ω was about 20 J/cm^2 and 5 J/cm^2, respectively. The optical uniformity of the sample was adequate to perform the measurements but distortion of the intensity profile of the propagating beam, especially the 3ω beam, was evident.

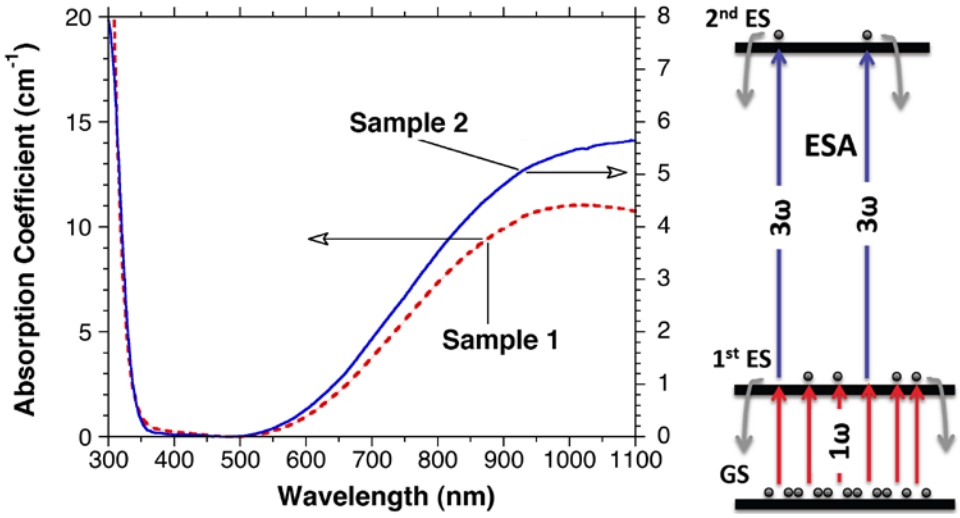

Fig. 2. Absorption spectra of the Fe-doped samples used in this work and schematic depiction of the basic excitation mechanisms involving linear absorption of 1ω photons from the ground state (GS) to the 1st excited state (1st ES) and excited state absorption of 3ω photons.

The absorption spectra of the two samples studies in this work are shown in Figure 2. Both exhibit similar spectral characteristics owning to the presence of Fe^{2+} ions. A strong absorption in the near infrared spectral region, and in particular at 1ω, is observed suitable for the use of this type of material for blocking the fundamental frequency of high power laser systems. On the other hand, the ultraviolet absorption edge is very close to the third harmonic (351) giving rise to an unacceptable level of absorption at 3ω. As a result, these two materials are not ideal for the intended application as they would induce transmission losses at 3ω via linear absorption mechanisms. However, we postulate that with proper future modifications of the base glass, the linear absorption at 3ω can be eliminated. However, the excited state absorption effect will be minimally affected unless the UV absorption edge is blue-shifted by more than about 1 eV since it is originated from linear absorption of 3ω photons by electrons that are transiently occupying the 1st excited state after they absorbed a 1ω photon. For clarity, this process is depicted as inset in Figure 2.

The absorption spectra shown in Figure 2 exhibit the characteristic spectral features of Fe^{2+} ions while there is no evident spectral signature of the presence of Fe^{3+} ions (such as absorption bands in the 350-500 nm spectra range). As it will be discussed elsewhere, the oxidation state of the dopant Fe ions is controlled by the co-dopant SnO and C. However, under excitation of our sample with 355 or 514 nm, a weak emission with a characteristic to Fe^{3+} ions peak centered at about 700 nm is observed indicative that a small Fe^{3+} ion concentration is present in our sample. Such emission in the NIR spectral region from Fe^{3+} ions has been reported in other similar systems such as in fluorozirconate glass [16]. We do not expect this population to affect our measurement as the Fe^{3+} ions will not induce absorption at 1ω but only contribute to linear absorption at 3ω which is considered as background in our measurements.

The experiments were designed to study parasitic nonlinear effects during operation of these materials under exposure to high power excitation conditions with the material used to block the 1ω light but allow the 3ω light to propagate unaltered. In such excitation conditions, the number of impurity ions available to absorb the 1ω photons (under practically optimal doping levels and material thickness on the order of 1 cm) is about one order of magnitude higher than the number of photons designated to absorb. Consequently, transient photo-bleaching effects during the laser pulse are possible which can affect the ability of the material to absorb the 1ω pulse In addition, absorption of 1ω photons leads to population of the first excited state which can subsequently support absorption of 3ω photons (excited state absorption) thus generated unwanted loss of 3ω laser power.

Based on the above discussion, we designed experiments to measure photo-bleaching and ESA absorption in these materials under exposure to 1ω and 3ω nanosecond high power laser pulses on the order of 10 J/cm^2. The photo-bleaching experiments involved the exposure of the samples to the 1ω laser beam and measuring the transmittance of the 1ω as a function of the 1ω input power. The excited state absorption experiments involved measuring the transmittance of the 3ω beam while varying the fluence of the 1ω beam while the two beams were overlapped. The smaller radius of the 3ω beam at the sample compared to the 1ω beam ensured that the 3ω beam is at nearly peak fluence of the 1ω beam while propagating through the sample.

Experimental results

To experimentally evaluate the presence of ESA in the samples used in this study, the experiments were performed in two steps. In step 1 we examined the presence of ESA by altering the 1ω fluence between high and low values while monitoring the transmittance through the sample of a lower power (≈100 mJ/cm^2) 3ω pulse aligned to co-propagate and spatially overlapped with the 1ω pulse as detailed in the experimental system section. This approach also allowed us to evaluate the optical stability of the sample, such as alteration of beam propagation due to laser induced damage or self focusing [17] and loss of transmission due to surface modification or bulk solarization (formation of color centers), under the experimental conditions. If it was determined that the optical stability of the sample was sufficient (as with the samples used in this work), we subsequently measured in step 2 the dependence of the transmittance at 3ω (due to ESA) as a function of the 1ω fluence.

Typical experimental results are presented in Fig. 3. Specifically, Fig. 3a shows the transmittance of the 3ω beam (measured for each individual pulse) propagating through sample 1 while the fluence of the co-propagating 1ω beam was altered between 0 and 5.5 J/cm^2. To improve statistics, the 1ω fluence was kept constant for about 20 pulses during which the average transmittance of the 3ω beam (pulses) during propagation through the sample was estimated. The results shown in Fig. 3a demonstrate a dependence in the observed transmittance at 3ω on the fluence of the co-propagating 1ω pulses. Specifically, the presence of the 1ω pulses cause a decrease in the transmittance (high absorption) of the 3ω pulse, which may be interpreted as originating in the presence of ESA. The results suggest that the ESA causes a decrease in transmittance of about 0.01 (1%) when the peak 1ω fluence is about 5.5 J/cm^2. Similar results were obtained from multiple sites and using various combinations of high and low 1ω laser fluences.

However, exposure of the sample to 1ω fluences above about 5.5 J/cm^2 yields instabilities in the baselibe transmittance at 3ω in this sample. This effect is assigned to a degradation/modification of the surface quality due to its interaction with the 1ω pulses. We have not examined the exact cause of this degradation as these samples are experimental and surface quality issues were not part of this investigation. It must be noted that the baseline transmittance of about 0.605 (60.5 %) is due to the losses from reflections on the sample's surface as well as absorption induced by the UV absorption edge of the sample that extends through 3ω as discussed in the previous sections.

The second sample (sample 2) used in this investigation exhibited much better optical stability as a function of the 1ω fluence as well as lower baseline absorption at 3ω. As a result, the change of the transmission at 3ω as a function of the 1ω fluence was experimentally measured in more detail. In this set of experiments, 1ω fluences up to about 15 J/cm^2 were utilized to capture the dependence of the 3ω transmittance as a function of the 1ω fluence. Typical experimental results are shown in Fig. 3b. These results were obtained after averaging the transmittance of 20 pulses at 3ω for each setting of the 1ω fluence. The results indicate a nearly linear behavior of the transmittance at 3ω as a function of the 1ω fluence over the range of fluences used in these experiments. For direct comparison with the results shown in Fig. 3a, the results of Fig. 3b suggest that the ESA is on the order of 3 % when the peak 1ω fluence is about 5.5 J/cm^2 compared to about 1.7 % observed in the mixed alkali-silicate glass sample. Experimental errors in the data arise mainly from small variations in the baseline transmission at 3ω between neighboring sites (within distances of about 100 μm) in combination with the beam stability (issue discussed in the experimental section), which is largely removed by averaging experimental over about 20 nominally identical measurements to obtain each experimental data point shown in Fig. 3.

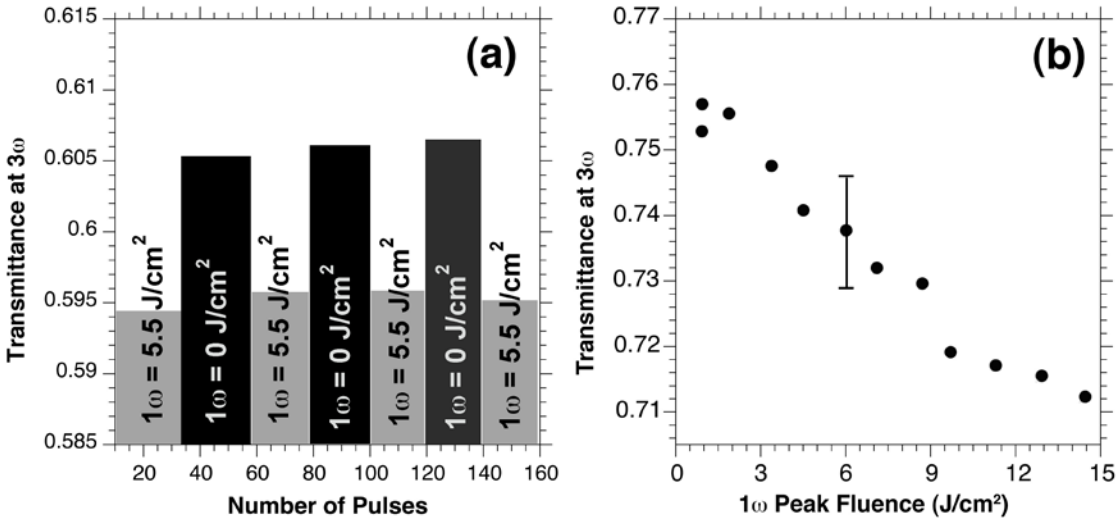

Fig. 3. The measured transmittance of the 3ω beam through a) sample 1 under simultaneous exposure to alternating 1ω fluence between a higher and a lower value and b) through sample 2 as a function of the 1ω fluence.

The high 1ω excitation conditions used in these experiments can lead to depletion of the ground state electrons (photo-bleaching) that are responsible for the absorption of the 1ω photons and consequently a reduction of the absorption coefficient during the laser pulse. Specifically, considering that a 1ω laser pulse having fluence of about 6 J/cm^2 is associated with 3.2 x10^{19} photons/cm^2 and the doping of the material (assuming an optimized optic with thickness of 1 cm) is on the order of 10^{20} Fe ions/cm^2, it becomes apparent that there is only a small number of Fe for each photon to be absorbed. Assuming the lifetime of the excited state is much longer than the pulse duration, there will be a continuous reduction, during the laser pulse, of the available Fe ions to absorb the photons, and a corresponding reduction in the absorption coefficient (photo-bleaching).

The studies of photo-bleaching were performed using sample 2 due to its higher resistance to optical modification (surface modification or damage effects that interfered with the acquisition of the data), for fuenses up to about 15 J/cm^2 at 1ω. Figure 4 shows representative results capturing the change of the measured transmittance at 1ω as a function of the peak fluence of the 1ω pulse. As with the previous measurement (see Fig. 3), each data point represents an average value over about 20 identical measurements.

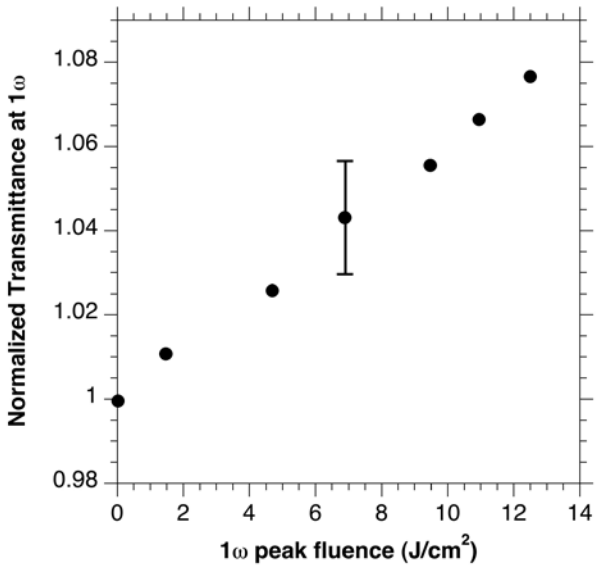

Fig. 4. The normalized transmittance of the 1ω pulsed beam propagating through the mostly Fe^{2+}-doped Lithium Sodium Silicate glass sample 2 as a function of the 1ω pulse peak fluence.

The results shown in Fig. 4 indicate a practically linear behavior of the transmission at 1ω as a function of the 1ω fluence over the range of fluences used in these experiments. Since the results were obtained and averaged over the entire spatially Gaussian beam, the transmission of 6 J/cm^2 spatially flattop beam (similar to that typically employed in large aperture laser systems) should be similar to about 12 J/cm^2 peak fluence for the beam profile used in this experiment. The observed transmission increase is about 7%.

Analysis and Discussion

As the estimated Fe^{2+}doping level of the material is about $4 \times 10^{20}/cm^3$ or about 1.136×10^{20} ions/cm^2 for the sample used for the measurement. The absorption coefficient of the material at 1ω (1064 nm) is about 5.59 cm^{-1} and the observed transmission increase of about 7% is equivalent to a decrease of the absorption coefficient to about 5.35 cm^{-1} which equivalent to passivation of about 4.3% of the Fe^{2+} ions or about 4.9×10^{18} ions/cm^2. But because the measurement represents an average value over the entire duration of the laser pulse, the estimated number of passivated Fe^{2+} ions at the end of the pulse should be about twice the average number (or about 9.8×10^{18} ions/cm^2.), if we assume that the lifetime of the excited state is significantly longer than the pulse duration, otherwise this number is smaller. In comparison, the number of photons propagating through the material for a 12 J/cm^2 peak fluence 6 J/cm^2 avearge fluence) used in this experiment is about 3.17×10^{19} photons/cm^2 and about 2.48×10^{19} photons/cm^2 are eliminated (using as absorption coefficient the estimated value of 5.35 cm^{-1}). The fact that the number of eliminated photos (2.48×10^{19}) is about 2.5 times the maximum estimated number of passivated Fe^{2+} ions (9.8×10^{18} ions/cm^2), it can be concluded that the lifetime of the first excited state (responsible for the 1ω absorption) is shorter than the duration of the laser pulse.

The pasivated Fe^{2+} ions are associated with ions that have absorbed one 1ω photon and therefore, their electron may occupy the 1^{st} exited state (see inset in Fig. 2) and be available to participate in ESA via the absorption of a 3ω photon. The absorption coefficient of this sample at 3ω (355 nm) is 0.193 cm^{-1} (see Fig. 2) while the results of Fig. 3b indicate that exposure to 12 J/cm^2 peak fluence at 1ω results to a decrease of the measured transmittance at 3ω of about 0.035, equivalent to an absorption coefficient of about 0.383 cm^{-1}. Assigning the difference on the absorption coefficient (0.19) to the ESA and normalizing by the average density of passivated ions (4.3% of the Fe^{2+} ions) yields an estimated average (during the laser pulse) value of the ESA absorption cross section of 1.1×10^{-20} cm^{-2}. For comparison, the linear absorption cross section at 1ω is about 1.4×10^{-20} cm^{-2}.

The samples used in this study were experimental, developed as part of a related study to develop a better understanding on how to control the redox state and UV absorption edge in Fe-doped glass systems. This work will be reported elsewhere [15]. The host material is not ideal for the intended application (as a red blocker in high power laser systems) mainly because there is still residual absorption at the third harmonic due to the fact that the UV absorption edge is not sufficiently blue shifted. Such blue shifting of the UV absorption edge would require a different glass matrix. For the materials used in this study, excited state absorption of a 3ω photon initiates transition of electrons deep in the charge transfer UV absorption band. Therefore, even if the UV absorption edge is sufficiently blue shifted to avoid any significant absorption at 3ω, excited state electrons can still absorb 3ω photons (via ESA) to reach the UV absorption bands. Consequently, we postulate that understanding the strength of the ESA process in these (non-optimized) materials can help provide an initial validation of the feasibility of developing such material with optimized performance and obtain an initial estimate of the expected operational parameters. Ideally, the UV absorption edge must be blue-shifted by more

than about 1 eV so that 3ω ESA transitions cannot reach the charge transfer UV absorption bands.

The photo-bleaching effect (reduction of the absorptivity of the material with increased 1ω fluence) arises from the generation of an exited state electron population and will be an issue independent of the base glass used or the location of the UV absorption edge. The results presented in this work attempt to quantify this effect which also helps provide estimates of the ESA cross section. This information may be used to assess other base materials and doping parameters to meet the requirements and system specifications

Acknowledgments

This work was performed under the auspices of the U.S. Department of Energy by Lawrence Livermore National Laboratory under Contract DE-AC52-07NA27344. [LLNL-JRNL-663392]

References

1. J. H. Campbell, J. S. Hayden, A. Marker, "High-Power Solid-State Lasers: a Laser Glass Perspective", Int. J. Appl. Glass Sci. 2, 3-29 (2011)
2. W. B. White, M. Matsumura, D. G. Linnehan, T. Furukawa, B. K. Chandrasekhar, "Absorption and luminescence of Fe3+ in single-crystal orthoclase", Am. Miner. 71, 1415-1419 (1986)
3. V. K. Khalilov, S. S. Pivovarov, "Fundamental absorption edge in vitreous silicas containing impurity iron", Sov J Glass Phys Ch+ 5, 408-413 (1979)
4. V. K. Khalilov, S. S. Pivovarov, V. K. Zakharov, N. M. Bokin, T. I. Prokhorova, E. V. Klimashina, B. S. Gorovaya, "Absorption spectra and structural state of Fe3+ ion in vitrous silicas and quartz" Sov J Glass Phys Ch+ 4, 155-159 (1978)
5. D. Ehrt , "UV-absorption and radiation effects in different glasses doped with iron and tin in the ppm range", C R Chim. 5, 679-692 (2002)
6. D. Ehrt , M. Leister, A. Matthai , "Polyvalent elements iron, tin and titanium in silicate, phosphate and fluoride glasses and melts", Phys. Chem. Glasses 42, 231-239 (2001)
7. K. E. Fox , T. Furukawa , W. B. White , "Transition-metal ions in silicate melts .2. Iron in sodium-silicate glasses", Phys. Chem. Glasses 23, 169-178, (1982)
8. L. B. Glebov , E. N. Boulos , "Absorption of iron and water in the Na2O-CaO-MgO-SiO2 glasses. II. Selection of intrinsic, ferric, and ferrous spectra in the visible and UV regions", J Non-Cryst Solids 242, 49-62 (1998)
9. H. Schirmer , M. Muller, C. Russel , "High-temperature spectroscopic study of redox reactions in iron and arsenic-doped melts", Glass Sci. Technol. 76, 49-55 (2003)
10. M. Yamashita, T. Akai, R. Sawa, J. Abe, M. Matsumura, "Effect of preparation procedure on redox states of iron in soda-lime silicate glass", J Non-Cryst Solids 354, 4534–4538, (2008)
11. R. K. Kukkadapu, H. Li, G. L. Smith, J. D. Crum, J. S. Jeoung, W. H. Poisl, M. C. Weinberg, "Mossbauer and optical spectroscopic study of temperature and redox effects on iron local environments in a Fe-doped (0.5 mol% Fe2O3) 18Na(2)O-72SiO(2) glass", J Non-Cryst Solids 317, 301-318 (2003)
12. V. K. Khalilov, S. S. Pivovarov, V. K. Zakharov, "The coordination of Fe2+ in Fe-doped crystalline and vitreous SiO2", Sov J Glass Phys Ch+ 2, 482-485 (1976)
13. V. K. Khalilov, S. S. Pivovarov, V. K. Zakharov, "The absorption spectra of the Fe 2+ ion in polarized light and its structural position in single-crystal quartz and in vitreous silica", Sov J Glass Phys Ch+ 3, 298-301 (1977)
14. T. T. Volotinen, J. M. Parker, P. A. Bingham, "Concentrations and site partitioning of Fe2+ and Fe3+ ions in a soda-lime-silica glass obtained by optical absorbance spectroscopy", Phys Chem Glasses-B 49, 258-270 (2008)
15. R. K. Brow et al. in preparation
16. E. Snow, J. A. Freitas, Jr., U. Strom, "Time-resolved photoluminescence of Fe3+ ions in fluorozirconate glass", Phys. Rev. B 37, 10332 (1988)
17. S. G. Demos, P. R. Ehrmann, M. A. Johnson, K. I. Schaffers, A. M. Rubenchik, M. D. Feit, "Change of self-focusing behavior of phosphate glass resulting from exposure to ultraviolet nanosecond laser pulses", Opt. Express, 21, 4854 (2013)